Journal of Power Sources 190 (2009) 25–33

Contents lists available at ScienceDirect

Journal of Power Sources

journal homepage: www.elsevier.com/locate/jpowsour

Analysis of the electrochemical behaviour of polymer electrolyte fuel cells using simple impedance models

Michael A. Danzer*, Eberhard P. Hofer

Institute of Measurement, Control and Microtechnology, Ulm University, Albert-Einstein-Allee 41, 89081 Ulm, Germany

ARTICLE INFO

Article history:
Received 12 June 2008
Received in revised form
25 September 2008
Accepted 1 October 2008
Available online 11 October 2008

Keywords:
Fuel cell
Impedance models
Electrochemical impedance spectroscopy

ABSTRACT

The analysis of the electrochemical behaviour of polymer electrolyte fuel cells (PEFC) both in time and frequency domain requires appropriate impedance models. Simple impedance models with lumped parameters as resistances and capacitances or Warburg impedances do have limitations: often the validity is limited to a certain frequency range, effects at very low or very high frequencies can not be described properly.

However, these models have their usefulness for engineering applications, e.g. to distinguish the major loss terms, to estimate the membrane resistance, and to observe the changes of internal losses of fuel cells over time without the need for additional sensors.

The work discusses different impedance configurations and their applicability to impedance spectra of a fuel cell stack. Impedance spectra at points along the DC polarization curve, as well as spectra at various operating conditions are analysed and identified by a complex nonlinear least squares method. Finally, the connection of the impedance data with and the assignment of the parameters to physical phenomena are discussed. The examination shows that simple impedance models are well qualified to describe the electrochemical behaviour over a wide frequency range at all operating conditions.

1. Introduction

The static IV-characteristics of a polymer electrolyte fuel cell shows a nonlinear behaviour. The major losses occurring in the electrochemical reaction are due to the charge transfer through electrode–electrolyte interfaces, the transport of gases through the porous layer and the conduction of protons through the polymer electrolyte membrane. The losses and their dependency on the current density, as depicted schematically in Fig. 1, are theoretically described and modelled in terms of overvoltages [1,2].

Nonetheless, a distinction of the single processes and their contribution to the overall losses is not possible by static measurements. IV-characteristics do not provide an insight in the fuel cell. To describe the dynamic electrochemical behaviour of a fuel cell and to distinguish single loss factors, further information and dynamic measurements are needed.

For the characterisation of the current state of a fuel cell, measurable states as pressures, temperature, and mass flows are available which are measured at the inlet or outlet of the fuel cell. Furthermore, the load current and the resulting fuel cell voltage are known. Internal loss terms which are crucial for the resulting voltage and therewith for the efficiency of the fuel cell cannot be measured directly. Hence, for the operation and development of fuel cells methods are required which provide information on internal losses and thereby enable an analysis of the processes taking place inside the fuel cell. For the operation of fuel cells information on the gas supply, on the humidification of the proton conducting membrane, and on transport hindrances are needed. For the production of fuel cells occurring ohmic resistance of membranes and electron conducting components need to be measured and validated. For the development of fuel cells processes leading to degradation need to be analysed.

An approach which gives an insight in the fuel cell stack is the analysis and identification of the fuel cell impedance [3]. The impedance $Z_{FC}(j\omega)$ can be regarded as the complex, nonlinear, frequency-dependent internal resistance of the fuel cell. The impedance of a fuel cell incorporates detailed information on the intrinsic loss factors, on the conductivity of the membrane, on the electrode processes, and on kinetic losses [4]. The measurement of the impedance spectrum at an operating point and the identification of an appropriate impedance model enable the desired distinction of loss terms, and a description of the dynamic electrochemical behaviour of a fuel cell.

* Corresponding author. Tel.: +49 731 5026325; fax: +49 731 5026301.
E-mail address: michael.danzer@uni-ilm.de (M.A. Danzer).
URL: http://www.uni-ulm.de/en/in/mrm/html (M.A. Danzer).

0378-7753/$ – see front matter © 2008 Elsevier B.V. All rights reserved.
doi:10.1016/j.jpowsour.2008.10.003

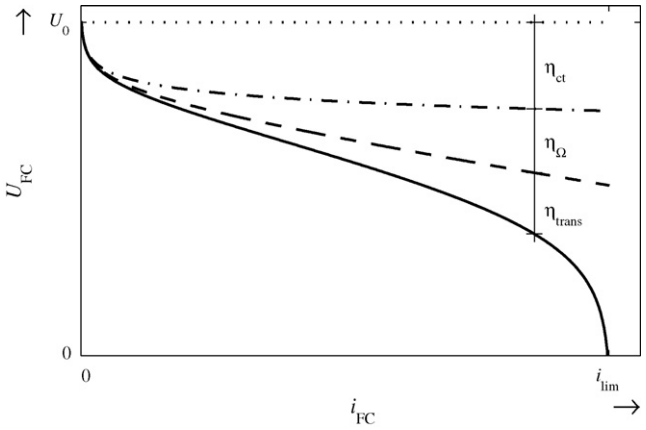

Fig. 1. IV-characteristics of a polymer electrolyte fuel cell with charge transfer overvoltage η_{ct}, ohmic overvoltage η_Ω, and transport overvoltage η_{trans}.

The most widely used method for analysing impedances is the electrochemical impedance spectroscopy (EIS). The approach of EIS is to measure impedances by applying successively single-frequency currents to the system and measuring the real and imaginary parts of the resulting voltage at that single frequency. Measuring the frequency response yields an impedance spectrum which can be modelled by an equivalent circuit, and identified by nonlinear complex parameter identification.

In the following, appropriate impedance models for PEFC are presented. Using these models, the electrochemical behaviour of a fuel cell stack is analysed by measuring impedance spectra at different operating conditions and by identification of the model parameters.

2. Impedance models

2.1. Contributions to the fuel cell impedance

Impedance spectra of fuel cell stacks are a superposition of various intrinsic loss factors and transient processes. Or in the words of an electrochemist: "A multitude of fundamental microscopic processes take place throughout the cell when it is electrically stimulated and, in concert, lead to the overall electrical response" [5]. These processes include the transport of electrons through the conductors, the transport of protons through the electrolyte, the transfer of electrons or ions at the electrode–electrolyte interfaces, and kinetic losses. In measured impedance spectra these processes are not imaged separately. What can be observed measuring an impedance spectrum are dissipative, capacitive, and inductive effects. Finally, by interpreting an impedance spectrum, these observations can be assigned to dominant physical processes. Dissipative effects can be assigned to the ohmic losses of the electron and proton conductance. Capacitive effects occur due to the double layers of the electrode–electrolyte interfaces. The dynamics of mass transport is imaged in an impedance spectrum as a conductive loop. Inductive effects appear due to the inductance of the cables.

A difficulty in interpreting impedance spectra is that besides single physical effects the impedance spectra of half-cells superpose to the impedance spectra of a single cell and the impedance spectra of single cells to the impedance spectrum of a fuel cell stack. Reversely, impedance spectra of fuel cell stacks always incorporate valuable information on the homogeneity of the single cells.

The purpose of an impedance characterisation of a fuel cell stack cannot be to reproduce all microscopic effects. The purpose of the following impedance analysis is to determine the essential properties and dominant loss factors of the fuel cell stack, their interrelations and their dependence on controllable variables as humidification, conversion, and current density.

2.2. Impedance modelling

Impedance models consist of a mathematical structure and therein incorporated parameters which are constant for a constant operating point but can vary for different operating points. Impedance models can be classified as process models and measurement models [6]. Process models are based on the mathematical description of physical phenomena and therefore incorporate physically meaningful parameters which can be identified by measurement and optimisation. In contrast, measurement models are mathematical structures with shapes that fit to measured impedance spectra. Their parameters do not directly have a physical meaning. But, by identifying the parameters for different operation conditions physical phenomena can be assigned.

The goal of the following impedance modelling is to find a model with a concise mathematical structure which regards the dominant effects and reflects the essential properties of the electrochemical system. To enable an interpretation of the model parameters and to guarantee a comparability of identified impedance spectra, the impedance model should include a minimum number of parameters and should yield a minimum error in between the modelled and the measured spectra.

Fig. 2 shows a typical impedance spectrum of a polymer electrolyte fuel cell. It is the Nyquist plot of a five cell stack with an active surface of 100 cm^2, a commercially available membrane electrode assembly with Pt/Ru and the gas diffusion layer SGL 10BB. The spectrum was measured at a current density of 0.5 A cm^{-2} with a minimum frequency of f_{min} = 0.2 Hz, and a maximum frequency of f_{max} = 10 kHz.

The impedance spectrum corresponds to the frequency response of the fuel cell at an operating point of the IV-characteristics. The task of modelling the impedance is to find a mathematical model which has a frequency response with the same shape and size or respectively, to find an equivalent circuit which shows the identical electrical behaviour.

2.3. Impedance elements

The basic elements for describing impedances are ohmic resistances R, capacitances C and inductances L with their complex resistances: $Z_R = R$, $Z_C = (j\omega C)^{-1}$ and $Z_L = j\omega L$. Consequently, intercepts of the positive real axis refer to ohmic resistances. A diverging

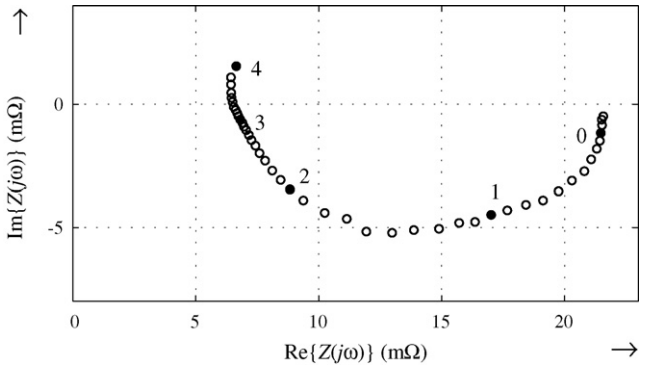

Fig. 2. Impedance spectrum of a PE fuel cell stack, five cells, A = 100 cm^2 at λ_C = 5 and λ_A = 1.43, i_{FC} = 0.5 A cm^{-2}, T_{Stack} = 55 °C, T_{DP} = 50 °C, f_{min} = 0.2 Hz, solid symbols denote decades of frequency.

impedance

$$\lim_{\omega\to\infty}\left\{Im\left\{Z(j\omega)\right\}\right\} = +\infty \quad (1)$$

refers to an inductance L.

Impedance arcs can be described by a combination of basic elements or by distributed elements. The following two combined elements are typical measurement models.

2.3.1. RC-circuit

An RC-circuit is a parallel connection of an ohmic resistance and a capacitance. The impedance of an RC-circuit

$$Z_{RC}(\mathrm{j}\omega) = \frac{R}{1+\mathrm{j}\omega\mathrm{RC}} \quad (2)$$

describes a semi-circle in the lower complex half-plane which is called a capacitive loop. As can be seen in Fig. 3(a), the impedance of the RC-circuit approaches the real axes for both limits, $\omega \to 0$ and $\omega \to \infty$, with an angle to the perpendicular of 0°. The product $\tau = RC$ is the time constant of the RC-circuit.

2.3.2. RLC-circuit

The RLC-circuit is the parallel extension of an RC-circuit by a series connection of a resistor R_b and an inductance L. Its impedance

$$Z_{RLC}(\mathrm{j}\omega) = \frac{R_aR_b + \mathrm{j}\omega R_aL}{R_a + R_b + \mathrm{j}\omega LR_aR_bC + (\mathrm{j}\omega)^2R_aL} \quad (3)$$

corresponds to a second order frequency response. The extension adds an inductive loop to the capacitive loop of the RC-circuit as shown in Fig. 3(b) [7].

The following distributed elements, the Nernst impedance Z_N and the generalised Warburg impedance Z_W, are process models describing diffusion processes.

2.3.3. Nernst impedance

The Nernst impedance

$$Z_N(j\omega) = r_N\frac{\tanh(\delta_N\sqrt{\mathrm{j}\omega/D})}{\sqrt{\mathrm{j}\omega\, D}} \quad (4)$$

with the diffusion coefficient D and the diffusion length δ_N describes the transport behaviour of the Nernst diffusion [8]. The static resistance of the of the Nernst impedance is

$$R_N = Z_N(0) = \lim_{\omega\to 0}\{Z_N(\mathrm{j}\omega)\} = \frac{r_N\delta_N}{D} \quad (5)$$

2.3.4. Warburg impedance

The generalised Warburg impedance

$$Z_W(\mathrm{j}\omega) = \frac{\tanh(R_W\alpha\sqrt{\mathrm{j}\omega})}{\alpha\sqrt{\mathrm{j}\omega}} \quad (6)$$

with the static resistance R_W can be regarded as a bounded constant phase element [9], or as a Warburg diffusion element [10], where α is a function of the diffusion coefficient and the diffusion length. The Warburg impedance approaches the origin for $\omega \to \infty$ with an angle to the real axes of 45° as depicted in Fig. 3(c).

2.4. Impedance models of a PE fuel cell

In Fig. 4 different impedance elements are assigned to the impedance spectrum of Fig. 2.

The intersection of the impedance spectrum with the real axis for $\omega \to \infty$ in Fig. 4 approximately corresponds to the ohmic resistance R_Ω, which is mainly due to the proton transport resistance of the membrane. The diverging impedance for $\omega \to \infty$ results from

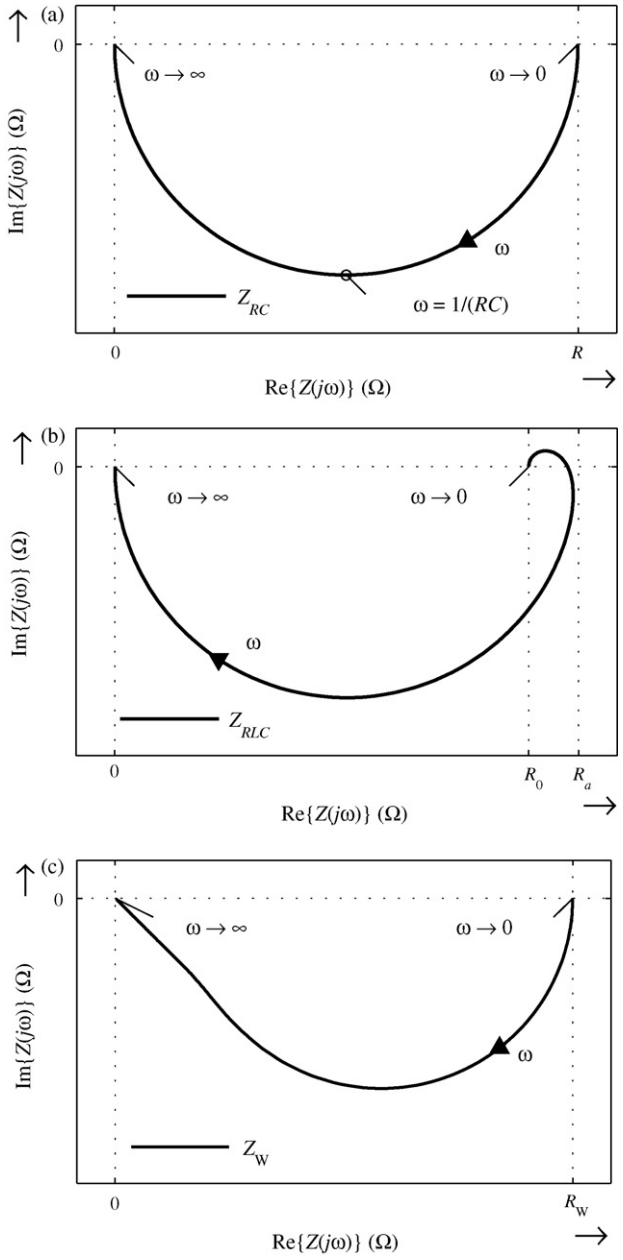

Fig. 3. Impedance spectra of elements. (a) Impedance spectrum of an RC circuit. (b) Impedance spectrum of an RLC circuit. (c) Impedance spectrum of a Warburg impedance.

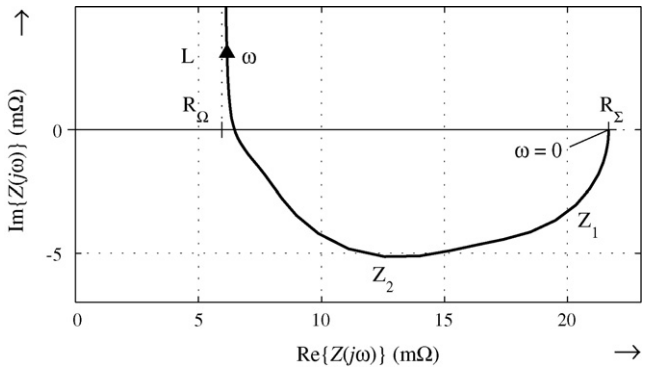

Fig. 4. Assignment of impedance elements to the impedance spectrum of Fig. 2.

the inductance of the cables, which is not an integral part of the fuel cell. For intermediate frequencies the impedance spectrum consists of two arcs, $Z_1(j\omega)$ and $Z_2(j\omega)$, which have to be examined in more detail later. In general, the impedance of a PEFC can be depicted as the series connection of the ohmic resistance R_Ω, two impedances Z_1 and Z_2 for the two arcs in the Nyquist plot and an inductance L. The resulting fuel cell impedance is

$$Z_{FC}(j\omega) = R_\Omega + Z_1(j\omega) + Z_2(j\omega) + Z_L(j\omega) \tag{7}$$

The intersection of the impedance spectrum with the real axis for $\omega \to 0$ corresponds to the static resistance

$$R_\Sigma = Z_{FC}(0) = \lim_{\omega \to 0} \{Z_{FC}(j\omega)\} \tag{8}$$

which is the limit value of the fuel cell impedance $Z_{FC}(j\omega)$ and can be calculated as the sum $R_\Sigma = R_\Omega + R_1 + R_2$, when R_1 and R_2 are the limit values of Z_1 and Z_2 for $\omega \to 0$.

In the following four impedance models of the PEFC are presented. These models have the ohmic resistance and the cable inductance in common and can be distinguished by the elements describing the two arcs in the Nyquist plot. Hence, the nomenclature depends on the impedance elements describing the impedance arcs.

The structure of the impedance models can be used for the whole operating range of a fuel cell. Identified parameters are only valid in a certain neighbourhood of an operating point.

The first two models, RC–RC and Randles, are well known in literature. The models RC–W and RLC–W were designed to fit the impedance spectra of the examined fuel cell.

2.4.1. RC–RC model

In the RC–RC model depicted in Fig. 5(a), the losses of the electron and proton conductance are described by an ohmic resistance and the two loops of the impedance spectrum each by an RC-circuit [11,12]. The impedance of the model is

$$Z_{RCRC}(j\omega) = R_\Omega + \frac{R_1}{1 + j\omega\tau_1} + \frac{R_2}{1 + j\omega\tau_2} + j\omega L \tag{9}$$

with the time constants $\tau_1 = R_1C_1$ and $\tau_2 = R_2C_2$ of the two RC-circuits. The series connection of an ohmic resistance and RC-circuits is also known as Voigt electrical circuit [6]. The parameter vector

$$\theta_{RCRC} = \begin{bmatrix} R_\Omega & R_1 & R_2 & C_1 & C_2 & L \end{bmatrix}^T \tag{10}$$

comprises the six parameters of the model. The static resistance equals the sum of the resistances.

This two-time-constants model has its limitations, e.g., when one limiting process is diffusion based. Depressed semi-circles and angles to the perpendicular to the real axes different from 0° cannot be described correctly. The RC–RC model can be regarded as the first approximation of the impedance of a PEFC.

2.4.2. Randles model

The Randles equivalent circuit in Fig. 5(b) describes the response of a single-step charge-transfer process with diffusion of reactants to the interface [10] and is often found in literature [3,9]. The equivalent circuit consists of an ohmic resistance R_Ω, a double layer capacity C_{dl} parallel to a series connection of a charge transfer resistance R_{ct} and a diffusion impedance Z_N. With the cable inductance the impedance is

$$Z_{Randles}(j\omega) = R_\Omega + \left[j\omega C_{dl} + (R_{ct} + Z_N(j\omega))^{-1} \right]^{-1} + j\omega L \tag{11}$$

The parameter vector

$$\theta_{Randles} = \begin{bmatrix} R_\Omega & R_{ct} & r_N & \delta_N & D & C_{dl} & L \end{bmatrix}^T \tag{12}$$

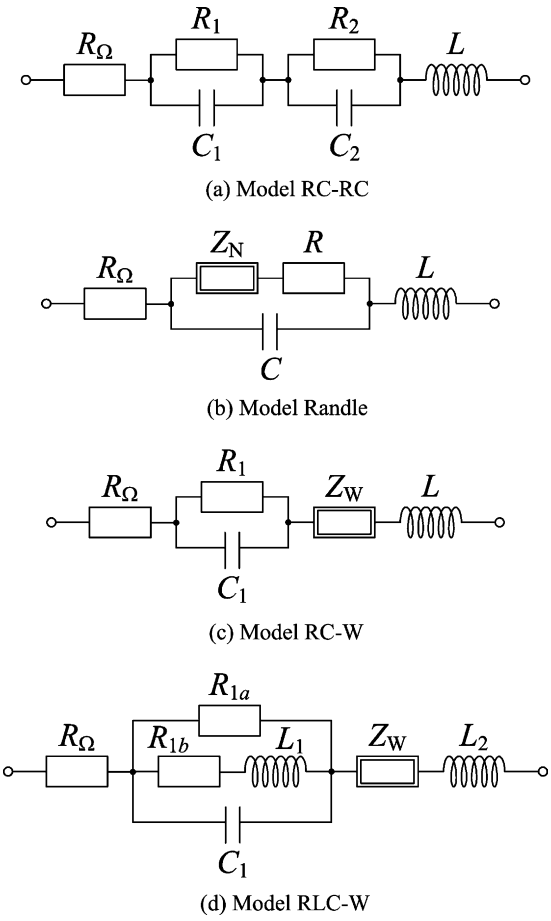

Fig. 5. Impedance models of a PEFC in the form of equivalent circuits.

comprises seven parameters. The static resistance is with (5)

$$R_{Randles} = R_\Omega + R_{ct} + R_N \tag{13}$$

The Randles model has the ability to describe depressed semi-circles. As the RC–RC model it has angles to the perpendicular to the real axes of 0°.

2.4.3. RC–W model

The RC–W model in Fig. 5(c) consists of an RC-circuit for the first impedance arc in the Nyquist plot for low frequencies and a Warburg impedance for the second. The impedance is

$$Z_{RCW}(j\omega) = R_\Omega + \frac{R_1}{1 + j\omega\tau_1} + Z_W(j\omega) + j\omega L \tag{14}$$

The parameter vector of the RC–W model

$$\theta_{RCW} = \begin{bmatrix} R_\Omega & R_1 & R_W & C_1 & \alpha & L \end{bmatrix}^T \tag{15}$$

consists of six parameters. As at the RC–RC model the static resistance equals the sum of the resistances.

The RC–W model is able, due to the Warburg impedance, to describe depressed semi-circles and has an angle to the real axes for $\omega \to \infty$ of 45°.

2.4.4. RLC–W model

If inductive effects occur in the impedance spectrum for small frequencies, the impedance element describing the first arc in the impedance spectra can be extended by an inductance. Hence the RLC–W model in Fig. 5(d) consists of an RLC-circuit for the first arc

and a Warburg impedance for the second:

$$Z_{\mathrm{RLCW}}(\mathrm{j}\omega) = R_{\Omega} + Z_{\mathrm{RLC}}(\mathrm{j}\omega) + Z_{\mathrm{W}}(\mathrm{j}\omega) + \mathrm{j}\omega L \tag{16}$$

The RLC–W model comprises eight parameters

$$\theta_{\mathrm{RLCW}} = \begin{bmatrix} R_{\Omega} & R_{1a} & R_{1b} & R_{\mathrm{W}} & C_1 & L_1 & \alpha & L_2 \end{bmatrix}^{\mathrm{T}} \tag{17}$$

The static resistance of the RLC–W model

$$R_{\mathrm{RLCW}} = R_{\Omega} + \frac{R_{1a}R_{1b}}{R_{1a}+R_{1b}} + R_{\mathrm{W}} \tag{18}$$

is the sum of the ohmic resistance, the Warburg resistance and the parallel connection of the resistances R_a and R_b.

3. Electrochemical impedance spectroscopy

The electrochemical impedance spectroscopy is an established and recognised frequency domain method for the characterisation of electrochemical systems. It is extensively described in literature [12–14] and widely used for the characterisation of fuel cell impedances [3,4,15–18].

The procedure of the EIS is

1. harmonic exctiation of the system at defined frequencies,
2. mesurement of the system response,
3. determination of the impedance at the current frequency,
4. parameter optimisation of the impedance model.

Modelling and parameter identification are integral parts of the method. The steps 1–3 are conducted for every single frequency.

In the application of the method for the analysis of fuel cells, the fuel cell current at a constant operating point is superimposed by a harmonic oscillation

$$I_{\mathrm{FC}} = I_{\mathrm{OP}} + a_i \sin(\omega t) \tag{19}$$

with the constant current I_{OP}, the amplitude a_i and the angular frequency ω. The current acts as system excitation; the resulting fuel cell voltage V_{FC} as system response. With its nonlinear IV-characteristics a fuel cell generally does not fulfil the Kramer–Kronig conditions which are linearity, causality, stability, and finiteness [9]. To meet the linearity conditions the amplitude a_i of the excitation signal needs to be small. On the other hand, the resulting voltage signal needs a minimum signal to noise ratio. Here, the amplitude of the current oscillation is chosen to 0.01 A cm^{-2}. Consequently to the nonlinearity of the system, impedance spectra of fuel cells are only valid in a neighbourhood of the operating point.

The advantage of the electrochemical impedance spectroscopy is the high accuracy of identified impedance models and its reliability. The main shortcomings are the long measurement time and the expensive measuring setup.

3.1. Hardware setup and execution of the test

For the measurement of the impedance spectra the Electrochemical Workstation IM6 and the electronic load EL300 from ZAHNER-Elektrik are used. With water cooling the electronic load has a maximum power of 300 W, a current range of 0–100 A and a frequency range of 10 mHz to 10 kHz. For the following analyses the frequency is logarithmically increased from 0.2 Hz to 10 kHz with 10 steps per decade.

Prior to an impedance measurement, the controllable states are set to their operating points and it is waited till the voltage signal reaches a stationary level and stays there for several minutes. The waiting time is 5–15 min, depending on the variations of the operating points.

3.2. Parameter identification

The task of the optimisation algorithm is to find the optimal set of parameters which minimises the error between the measured impedance data Z_{FC} and the model output $Z_{\mathrm{FC,mod}}(\theta)$. The according objective function of the parameter optimisation is defined as

$$J(\theta) = \sum_k \left(g_R\, e_{R,k}(\theta)\right)^2 + \sum_k \left(g_I\, e_{I,k}(\theta)\right)^2 \tag{20}$$

with the errors of the real and the imaginary part for every frequency ω_k

$$e_{\mathrm{R},k} = Re\left\{Z_{FC}(\mathrm{j}\omega_k)\right\} - Re\left\{Z_{FC,\mathrm{mod}}(\mathrm{j}\omega_k, \theta)\right\} \tag{21}$$

and

$$e_{\mathrm{I},k} = Im\left\{Z_{FC}(\mathrm{j}\omega_k)\right\} - Im\left\{Z_{FC,\mathrm{mod}}(\mathrm{j}\omega_k, \theta)\right\} \tag{22}$$

and the corresponding weighting factors $g_{\mathrm{R}} = 1$ and $g_{\mathrm{I}} = 2$.

As optimisation algorithm a coupled evolutionary algorithm [19–21] with the deterministic Nelder–Mead method [22] is used. The hybridisation of the stochastic with the deterministic method provides the possibility to combine the advantages of both types of methods [23]. The evolutionary algorithm performs the task of the global search. The Nelder–Mead method accelerates the convergence towards a minimum. Ultimately the convergence to the global minimum cannot be proven, but repeated experiments have yielded reliable and reproducible results.

4. Analysis of PE fuel cell impedance spectra

The model-based analysis of the electrochemical behaviour is conducted using a fuel cell stack with five cells, an active surface of 100 cm^2, a commercially available membrane electrode assembly with Pt/Ru and the gas diffusion layer SGL 10BB. The fuel cell is fed with hydrogen and compressed air, which is humidified by a dew point humidifier. All impedance spectra are measured at ambient pressure.

4.1. Comparison of the impedance models

4.1.1. Test 1

At a constant operating point the impedance spectrum of the fuel cell stack is measured. On the basis of the measured impedance spectrum the parameters of the models discussed in Section 3 are identified and compared. The operating point is determined by a current density of $i_{\mathrm{FC}} = 0.5$ A cm^{-2}, an excess ratio of oxygen and hydrogen of $\lambda_{\mathrm{O_2}} = 3.33$ and $\lambda_{\mathrm{H_2}} = 1.25$, a fuel cell temperature of $T_{\mathrm{FC}} = 55\,^{\circ}$C and a temperature of the dew point humidifier of $T_{DP} = 55\,^{\circ}$C.

4.1.2. Observation

Fig. 6(a) and (b) shows the Nyquist plot of the measured and modelled impedance spectra. Fig 7(a) and Fig. 7(b) shows the squared error, $e_k = e_{r,k} + e_{\mathrm{I},k}$, of the modelled spectra at every frequency. All four models are able to describe the measured impedance spectrum.

Both models with the Warburg impedance, RC–W and RLC–W, yield the lowest values of the objective function (20). The diagrams of the squared errors show that the models RC–RC, Randles and RC–W yield similar errors for small frequencies. Solely the RLC–W is able, due to the additional inductance, to reduce the error at small frequencies. At high frequencies the models with the Warburg impedance show lower errors, because the Warburg impedance leads to an angle to the perpendicular on the real axis of 45°.

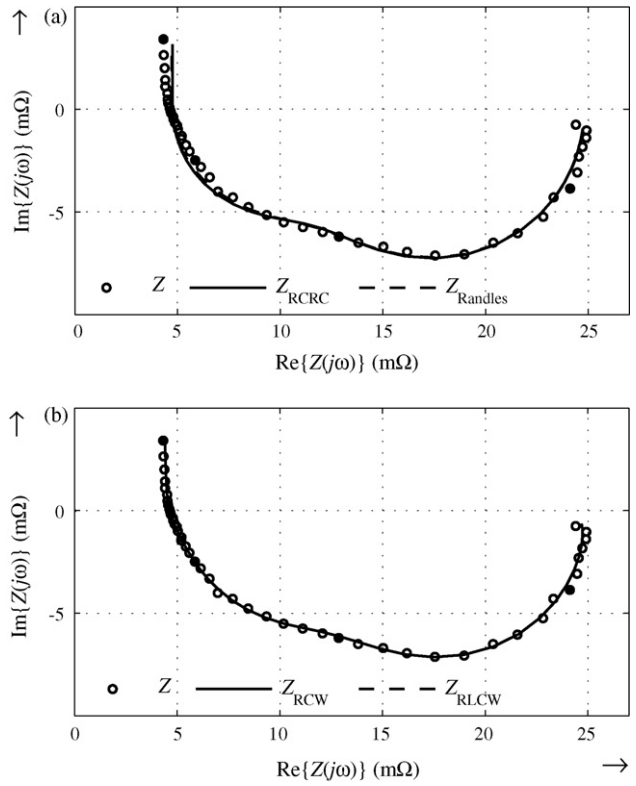

Fig. 6. Test 1: comparison of fuel cell impedance models. (a) Models RC-RC and Randles. (b) Models RC–W and RLC–W.

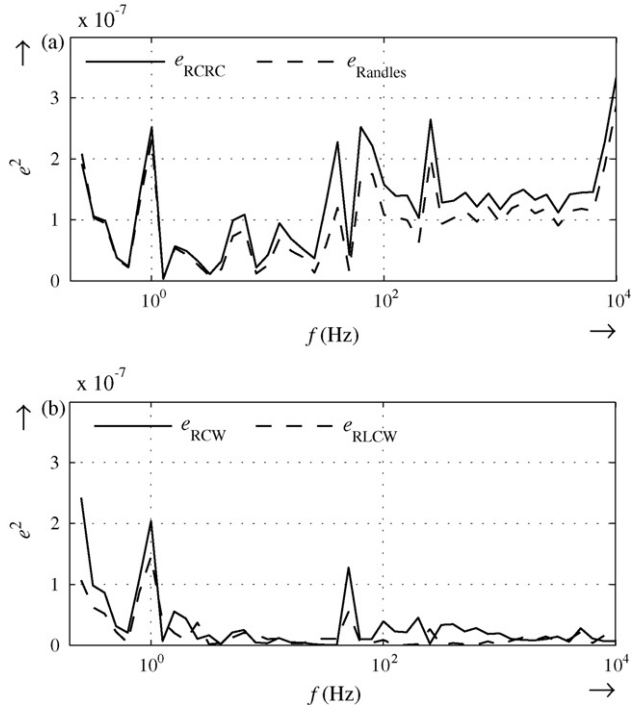

Fig. 7. Test 1: error structure of the comparison of the fuel cell impedance models (a) models RC-RC and Randles. (b) Models RC-W and RLC–W.

Table 1
Comparison of the identified resistances and the values of the objective function of the models RC–RC, Randles, RC–W und RLC–W. Here, R_1 and R_2 are the limit values of the first and the second impedance arc.

Model	R_Ω (mΩ)	R_1 (mΩ)	R_2 (mΩ)	R_Σ (mΩ)	J
RC–RC	4.76	12.9	7.14	24.8	6.84 e−6
Randles	4.72	12.3	7.74	24.8	5.66 e−6
RC–W	4.04	12.3	8.52	24.8	2.82 e−6
RLC–W	4.29	4.82	15.2	24.3	1.48 e−6

The static resistance R_Σ is identically identified for the models RC–RC, Randles and RC–W (see Table 1). The RLC–W yields a little smaller static resistance. The single resistances vary. Especially the ohmic resistance R_Ω is overestimated by the models RC–RC and Randles (Tables 2 and 3)

4.1.3. Results

The RC–W model meets best the requirements for the impedance modelling. It is able to fit the measured impedance spectrum, yields a very small error over the whole frequency range, and incorporates a minimum number of parameters. Therefore, it will be used for the following analysis at different operating points.

4.2. Impedance spectra along the IV-characteristics

4.2.1. Test 2

At defined operating points along the IV-characteristics the impedance spectra of the fuel cell stack are measured and identified using the RC–W model. The controllable states are set to $\lambda_{O_2} = 3.33$, $\lambda_{H_2} = 1.25$, $T_{FC} = 55\,^\circ$C and $T_{DP} = 55\,^\circ$C.

4.2.2. Observation

Fig. 8(a) and (b) shows the impedance spectra of the identified models at the defined operating points along the IV-characteristics. The ohmic resistance which almost coincides with the intercept of the impedance spectra with the real axis for high frequencies is equal for all operating points. The over-all resistance R_Σ decreases from 10 to 40 A, and from there on increases till the maximum current of 80 A. As can be seen in Fig. 8(a), for small currents the second impedance arc at high frequencies dominates. In contrast, Fig. 8(b) shows that for high currents the first impedance arc dominates.

Fig. 9 shows a diagram of the single parameters in dependency on the fuel cell current. It emphasises the observation that the ohmic resistance stays constant at constant humidification for all currents. The resistance R_1 of the RC-circuit which describes the first impedance arc for low frequencies increases with increasing current density. Whereas the resistance R_W of the Warburg impedance decreases.

Table 2
Identified resistance values of the RC–W model at varied hydrogen excess ratios.

λ_{H_2}	1.33	1.25	1.18	1.11
R_Ω (mΩ)	4.01	4.00	3.97	3.96
R_1 (mΩ)	12.4	13.1	13.5	15.2
R_W (mΩ)	9.18	8.87	9.22	8.98

Table 3
Identified resistance values of the RC–W model at varied oxygen excess ratios.

λ_{O_2}	4	3.33	2.86	2.5
R_Ω (mΩ)	4.03	3.99	3.97	3.98
R_1 (mΩ)	10.6	13.7	16.9	21.2
R_W (mΩ)	8.54	9.12	9.75	10.6

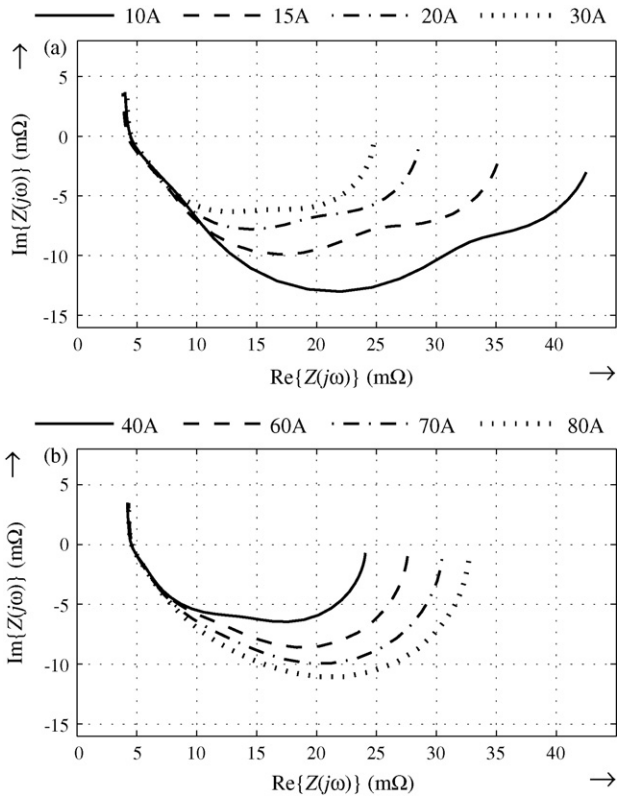

Fig. 8. Test 2: Impedance spectra at operating points along the IV-characteristics. (a) I = 10–30 A. (b) I = 40–80 A.

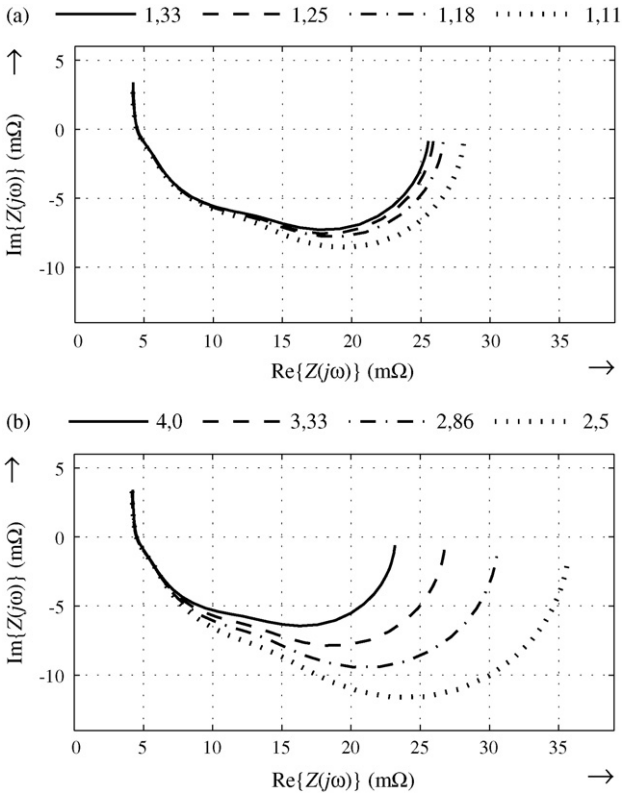

Fig. 10. Test 3: Impedance spectra at a varied excess ratio. (a) Hydrogen. (b) Oxygen.

4.2.3. Results

The structure of the RC–W model as measurement model is able to describe the impedance spectra over the whole current density range. Thereby, the identified parameters show a functional dependency on the fuel cell current. The decreasing resistance of the Warburg impedance and the increasing resistance of the RC-circuit with increasing current density link the parameters to the overvoltages of the static IV-characteristics. Thus, the RC-circuit is dominated by transport properties and the Warburg impedance by charge transfer phenomena. This result is in contradiction to the physical origin of the Warburg impedance; but it is in accordance to the results and assignments of the impedance arcs in [24]. Hence, the mathematical structure of the Warburg impedance is used as a measurement model to describe a different physical phenomenon than the diffusion.

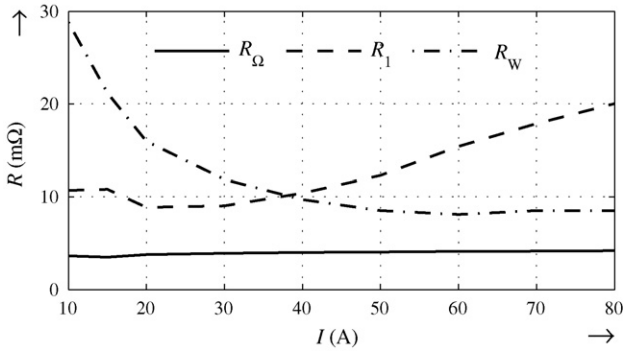

Fig. 9. Test 2: Identified resistances along the IV-characteristics.

The assignment of the impedance arcs shall be further analysed in the following tests.

4.3. Impedance spectra at a varied conversion of oxygen and hydrogen

4.3.1. Test 3

In the first test series the excess ratio of hydrogen, which is defined as the inverse of the conversion, is varied between λ_{H_2} = 1.33 and λ_{H_2} = 1.11 whilst the excess ratio of oxygen is kept constant at λ_{O_2} = 3.33. In the second test series the excess ratio of oxygen is varied between λ_{O_2} = 4 and λ_{O_2} = 2.5 whilst the excess ratio of oxygen is kept constant at λ_{H_2} = 1.25. The controllable states are set to i_{FC} = 0.5 A cm^{-2}, T_{FC} = 55 °C and T_{DP} = 55 °C.

4.3.2. Observation

Fig. 10(a) shows the impedance spectra at a varied hydrogen excess ratio. The intersection with the real axis and therewith the ohmic resistance as well as the second impedance arc for high frequencies stay unchanged for all different mass flows. The first impedance arc increases slowly with decreasing excess ratio. Fig. 10(b) shows impedance spectra at a varied oxygen excess ratio. Again, the second arc stays constant. The first arc increases rapidly with decreasing excess ratio.

4.3.3. Results

The increasing first impedance arc with decreasing excess ratio is in accordance to the results of the preceding test series, since a variation of the excess ratio primarily has an effect on the transport properties. A reduced incoming mass flow of the educts leads to a lower partial pressure at the active surface, to a reduced concentration gradient and therewith to higher transport losses. A varied excess ratio has less effect at the anode side with hydrogen than

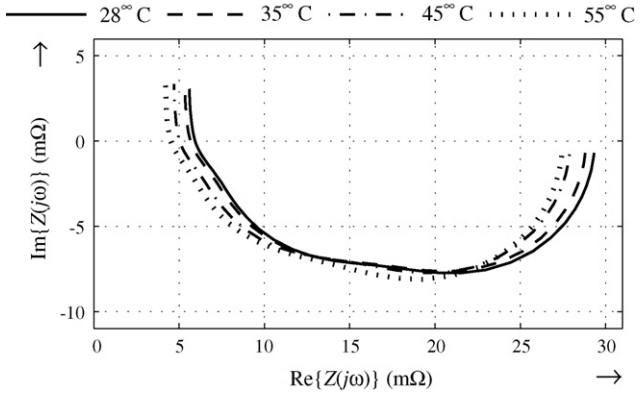

Fig. 11. Test 4: Impedance spectra at a varied humidification.

at the cathode with the oxygen in the air. At $\lambda_{H_2} > 1.11$ they are approximately negligible. The constant ohmic resistance implies that the fuel cell is sufficiently humidified for all excess ratios.

4.4. Impedance spectra at a varied humidification

4.4.1. Test 4

The dew point temperature in the humidifier is stepwise increased. Thereby, the relative humidity of the supplied air increases. The controllable states are set to $i_{FC} = 0.5\,A\,cm^{-2}$, $\lambda_{O_2} = 3.33$, $\lambda_{H_2} = 1.25$, and $T_{FC} = 55\,^{\circ}C$.

4.4.2. Observation

Fig. 11 shows the impedance spectra at a variation of the dew point temperature between $T_{DP} = 28\,^{\circ}C$ and $T_{DP} = 55\,^{\circ}C$. The last value is equal to the constant fuel cell temperature. The identified impedance spectra marginally change their shape and size. By varying the humidification they are solely horizontally shifted due to a decreased ohmic resistance with an increased water content of the membrane. This result is also reflected by the values of the parameters in Table 4. With increasing humidity in the fuel cell the transport hindrances and therewith the resistance of the RC-circuit increase, especially when the dew point temperature of the incoming air is higher than the fuel cell temperature.

4.4.3. Results

The observations emphasise the assumption that the ohmic resistance of the impedance models is mainly due to the proton transport through the polymer membrane with its water content dependent conductivity. The increasing resistance of the RC-circuit with increasing humidity again supports the result that the first impedance arc at low frequencies is dominated by transport properties.

4.5. Limitations of the impedance models

The RC–W model used in the preceding tests is well qualified to describe the dynamic behaviour of the fuel cell stack at very different operating conditions in the regarded frequency range, $f \in [0.2; 10e3]$ Hz. For frequencies beyond the regarded range no guaranteed statements can be made. If an inductive loop appears for frequencies lower than 0.2 Hz instead of the RC–W model the extended RLC–W models has to be used.

Besides the limitation of the model to the regarded frequency range, the applicability is limited to the measured current range, $I_{FC} \in [0; 80]$ A. Statements about the electrochemical behaviour at higher current densities are not guaranteed. But, the tests at very low stoichiometries indicate that the model is suited to describe the electrochemical behaviour at very high current densities, especially the occurring transport limitations.

Table 4
Identified resistance values of the RC–W model at a varied humidification.

T_{DP} (°C)	28	35	45	55	65
R_Ω (mΩ)	5.33	5.07	4.46	4.00	3.81
R_1 (mΩ)	12.3	12.1	12.6	13.5	15.9
R_W (mΩ)	11.7	11.6	10.9	9.98	9.62

5. Conclusion

A simple impedance model is found with a concise mathematical structure, a minimum number of six parameters and a minimum error to the measured impedance spectra. It is well qualified to describe all measured impedance spectra at very different operating conditions. By the identification of the model parameters at different test series physical phenomena were assigned. The identified values of the parameters at different operating conditions provide the possibility to determine the current state of the fuel cell, to distinguish the major loss terms and therewith to give an insight into the fuel cell.

The impedance model with the identified parameters and their physical interpretation are useful for engineering applications, e.g., to estimate the membrane resistance and for humidification control, to observe the changes of internal losses of fuel cells over time without the need for additional sensors, especially for lifetime and degradation testing. The model and an appropriate transformation into time domain can be used for online diagnostic methods [25,26].

Acknowledgement

The authors gratefully acknowledge the cooperation and support of the Center for Solar Energy and Hydrogen Research (ZSW) in Ulm, especially for the opportunity of using their test environment.

References

[1] J. Amphlett, R. Baumert, R. Mann, B. Peppley, P. Roberge, J. Electrochem. Soc. 142 (1995) 1–8.
[2] J. Kim, S. Lee, S. Srinivasan, J. Electrochem. Soc. 142 (1995) 2670–2674.
[3] B. Andreaus, A. McEvoy, G. Scherer, Electrochim. Acta 47 (2002) 2223–2229.
[4] J. Le Canut, R.M. Abouatallah, D.A. Harrington, J. Electrochem. Soc. 153 (2006) A857–A864.
[5] J.R. Macdonald, W.B. Johnson, Impdedance Spectroscopy: Theory, Experiment and Applications, John Wiley & Sons, 2005, pp. 1–26.
[6] P. Agarwal, M.E. Orazem, L.H. Garcia-Rubio, J. Electrochem. Soc. 139 (1992) 1917–1927.
[7] P. Piela, R. Fields, P. Zelenay, J. Electrochem. Soc. 153 (2006) A1902–A1913.
[8] B.H. Andreaus, Die Polymer-Elektrolyt-Brennstoffzelle-Charakterisierung ausgewählter Phänomene durch elektrochemische Impedanzspektroskopie (German), Ph.D. Thesis, EPF Lausanne, Switzerland, 2002.
[9] A. Lasia, Modern Aspects of Electrochemistry, Kluwer Academic/Plenum Publishers, 1999, Chapter 2: Electrochemical impedance spectroscopy and its applications, pp. 143–248.
[10] I.D. Raistrick, D.R. Franceschetti, J.R. Macdonald, Impedance Spectroscopy: Theory, Experiment and Applications, John Wiley & Sons, 2005, Chapter 2: Theory, pp. 27–128.
[11] J. Bauerle, J. Phys. Chem. Solids 30 (1969) 2657–2670.
[12] E. Ivers-Tiffée, A. Weber, H. Schichlein, Handbook of Fuel Cells: Fundamentals Technology and Applications, John Wileys & Sons, 2003, pp. 220–235.
[13] E. Barsoukov, J.R. Macdonald (Eds.), Impedance Spectroscopy: Theory, Experiment, and Applications, John Wiley & Sons, 2005.
[14] B.E. Conway, J.O. Bockris, R.E. White (Eds.), Modern Aspects of Electrochemistry, Kluwer Academic, 1999.
[15] A. Hakenjos, Untersuchung zum Wasserhaushalt von Polymerelektrolyt-membran-Brennstoffzellen (German), Ph.D. Thesis, Albert-Ludwig University Freiburg, Germany, 2006.
[16] H. Kuhn, In-Situ Charakterisierung von Polymer-Elektrolyt Brennstoffzellen mittels Elektrochemischer Impedanzspektroskopie (German), Ph.D. Thesis, ETH Zürich, Switzerland, 2006.
[17] N. Wagner, J. Appl. Electrochem. 32 (2002) 859–863.

[18] F. Richter, C. Schiller, N. Wagner, in Electrochemical applications: advances in electrochemical applications of impedance spectroscopy, Zahner-Elektrik (2002).
[19] J. Holland, SIAM J. Comput. 2 (1973) 88–105.
[20] I. Rechenberg, Evolutionsstrategie: Optimierung technischer Systeme nach Prinzipien der biologischen Evolution (German), Frommann Holzboog, 1973.
[21] D. Quagliarella, A. Vicini, Genetic Algorithms and Evolutionary Strategy in Engineering and Computer Science, John Wiley & Sons, 1998, Chapter 14: Coupling genetic algorithms and gradient based optimization techniques, pp. 289–310.
[22] J. Nelder, R. Mead, Comput. J. 7 (1965) 308–313.
[23] R. Chelouah, P. Siarry, Eur. J. Oper. Res 148 (2003) 335–348.
[24] I. Schneider, H. Kuhn, A. Wokaun, G. Scherer, J. Electrochem. Soc 152 (2005) A2092–A2103.
[25] L. Schindele, Einsatz eines leistungselektronischen Stellglieds zur Parameteridentifikation und optimalen Betriebsführung von PEM-Brennstoffzellensystemen (German), Ph.D. Thesis, University Karlsruhe, Germany, 2006.
[26] M.A. Danzer, E.P. Hofer, Electrochemical parameter identification: an efficient method for fuel cell impedance characterisation, J. Power Sources 183 (2008) 55–61.